Advances in Nano Research, *Vol. 16, No.6 (2024) 579-591*
https://doi.org/10.12989/anr.2024.16.6.579

Thermal radiation and some physical combined effects on an asymmetric peristaltically vertical channel of nanofluid flow

Amira S. Awaad[1,3a] and Zakaria M. Gharsseldien[*2]

[1]*Department of Mathematics, College of Science and Humanities in Al-Kharj Prince Sattam Bin Abdulaziz University, Al-Kharj 11942, Saudi Arabia*
[2] *Department of Mathematics, Faculty of Science, Al-Azhar University, Nasr City, Cairo, Egypt*
[3]*Department of Mathematics, Faculty of Science (Girls), Al-Azhar University, Nasr City, Cairo, Egypt*

(*Received September 22, 2023, Revised May 20, 2024, Accepted May 24, 2024*)

Abstract. This study explained the effects of radiation, magnetic field, and nanoparticle shape on the peristaltic flow of an Upper-Convected Maxwell nanofluid through a porous medium in an asymmetric channel for a better understanding of cooling and heating mechanisms in the presence of magnetic fields. These phenomena are modeled mathematically as a system of non-linear differential equations, that are solved under long-wavelength approximation and low Reynolds number conditions using the perturbation method. The results for nanofluid and temperature described the behavior of the pumping characteristics during their interaction with (the vertical position, thermal radiation, the shape of the nanoparticle, and the magnetic field) analytically and explained graphically. Also, the combined effects of thermal radiation parameters and some physical parameters on pressure rise, pressure gradient, velocity, and heat distribution are pointed out. Qualitatively, a reverse velocity appears with combined high radiation and Grashof number or combined high radiation and low volume flow rate. At high radiation, the spherical nanoparticle shape has the greatest effect on heat distribution.
Keywords: maxwell nanofluid; nanoparticle shape; peristaltic flow; thermal radiation

1. Introduction

Soon we will realize that the world of industrial engineering and biological sciences has been revolutionized by the advent of the use of nanofluids. Nanofluids e.g. oil, ethylene, methanol, etc. are prepared by dispersing nanometer-sized materials (approximately less than 100 nm) in base fluids. Nanofluids can increase convective heat transfer coefficient and the thermal conductivity compared to these conventional heat transfer fluids has been explained by Noreen (2018) and (Daryayehsalameh *et al*. 2022). The heat transmission properties of nanofluids make them a viable option for industrial and engineering applications such as heating, solar collectors, air conditioning (HVAC) systems, ventilation, refrigeration, etc. (Shah *et al*. 2022). Nanoparticle diameter, nanoparticle volume fraction, nanofluid temperature, base fluid thermal conductivity, and nanoparticle thermal conductivity, can directly influence the thermal conductivity of the nanofluid, (Rezaee *et al*. 2022) and (Kazemia *et al*. 2014). (Jafaripournimchahi *et al*. 2024) investigated the effect of thermal radiation and magnetic fields on mixed convection in a hybrid alumina–copper/ water nanofluid flowing over a permeable vertical flat plate.

Recently, researchers have done deeper work into the applications of nanofluids, they considered the phenomenon of peristalsis — the successive contraction and relaxation of a tube or channel wall, which has a lot of applications in the applied sciences. This includes biological systems like the movement of chyme in the gastrointestinal tract, the urine transport from the kidney to the bladder, movement of the ovum in the female fallopian tube, the vasomotion of small blood vessels such as arterioles, venules, and capillaries, swallowing of food through the esophagus, and transport of lymph in the lymphatic vessels. In industrial point of view, peristaltic flows play an important role in toxic liquid transport in the nuclear industry, sanitary fluid transport, transport of corrosive fluid, etc. (Gharsseldien *et al*. 2010). No doubt nanotechnology with peristalsis is a hot topic of research at present, peristaltic nanofluid flow has attracted the interest of scientists due to its applications. (Iqbal *et al*. 2023) studied the influences of heat and mass transfer on the peristaltic transport of Powell-Eyring nanofluid with MHD through a curved channel. (Hussain *et al*. 2023) investigated the effect of heat generation/ absorption on motile microorganisms and three-dimensional Darcy-Forchheimer nanofluid flow by a porous rotatable disk. (Ahmed *et al*. 2024) examined the attributes of heat and mass transfer on the peristaltic flow of a nanofluid within an asymmetric porous channel.

As a clear advance for research in this area, the effects of Hall currents and slip boundary conditions on peristaltic motion of a Bingham-Papanastasiou fluid model through an asymmetric channel, taking into account the heat generation, and thermal radiation, studied by (Eldabe *et al*. 2020). (Ahmed *et al*. 2021) analyzed the peristaltic motion in the symmetric channel under the influence of Hall current, magnetic field, and mixed convection of Powell-

*Corresponding author, Ph.D., Former Lecturer,
E-mail: gharsseldienz@gmail.com
[a] Ph.D., E-mail: a.asar@psau.edu.sa

ISSN: 2287-237X (Print), 2287-2388 (Online)

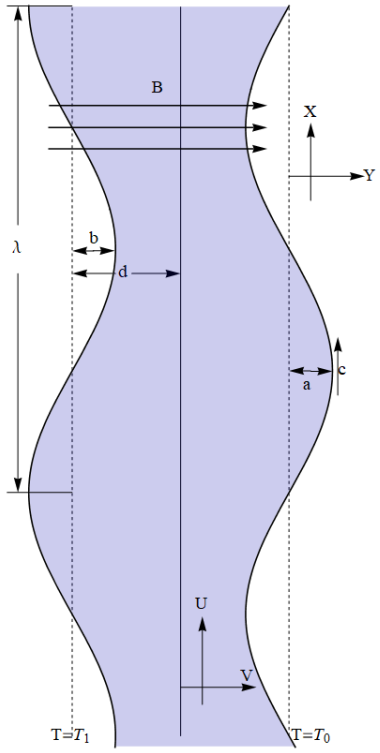

Fig. 1 Geometry of the problem

Eyring nanofluid. (Rafiq *et al*. 2019), examined the effects of ion slip and Hall on the peristaltic flow in a channel with compliant walls and viscous nanofluid. (Sharif *et al*. 2021) studied the effects of heat parameters, chemical reactions, and bioconvection phenomena in the MHD boundary layer flow of a non-Newtonian nanofluid with Cattaneo-Christov heat flux past a stretchable cylinder. (Ahmed *et al*. 2023) studied the effect of magnetic field on the peristaltic activity of Powell-Eyring through a flexible channel with nanomaterial, they take into account dissipation and Joule heating effects. (Mirzaei *et al*. 2023) investigated magnetohydrodynamic (MHD) heat and mass transfer phenomena on a circular cavity with a variable number of obstacles in each step. (Ahmadi Azar *et al*. 2023) introduced the effect of structural changes of two coaxial stretching disks in the heat and mass transfer with micropolar fluid.

There are also a lot of studies investigating the dynamics of Maxwell nanofluids whether with peristaltic motion or without it as: Gharsseldien and Awaad (2022), Azam (2022), Vijay and Sharma (2023) and (Kodi *et al*. 2023). The combined effect of thermal radiation with MHD in Maxwell nanofluids provides support for a better understanding of cooling and heating mechanisms in the presence of magnetic fields, which is relevant for electronic cooling systems (Zainal *et al*. 2022). In this paper we introduce theoretically, the combined effects of thermal radiation with some physical parameters on a magneto-Maxwell nanofluid flow through a porous medium in an asymmetric peristaltically vertical channel, computed results for pressure rise, pressure gradient, nanofluid velocity, and temperature distributions are obtained analytically and explained graphically.

2. Mathematical formulation

Consider the peristaltic transport of a two-dimensional flow of an incompressible Maxwell nanofluid with MHD and radiation through a porous medium in a vertical asymmetric channel. The peristaltic waves are traveling along the X- axis with speed c. Taking the two-dimensional cartesian coordinates (Y, X) where Y-axis is normal to it (Horizontal Axis) while X-axis is taken in motion direction (Vertical Axis) as shown in Fig. 1.

The basic equations of mass, momentum, and temperature introduced by (Vajravelu *et al*. 2011) and Sobamowo (2018), will be in the form

$$\nabla \cdot \boldsymbol{V} = 0, \tag{1}$$

$$\rho_{nf} \frac{d\boldsymbol{V}}{dt} = -\nabla P + \nabla \cdot \boldsymbol{S} + \boldsymbol{F}, \tag{2}$$

$$(\rho C)_{nf} \frac{dT}{dt} = k_{nf}\nabla^2 T + \boldsymbol{S} \cdot \nabla \boldsymbol{V} - \nabla \cdot \boldsymbol{q}_r, \tag{3}$$

$$\boldsymbol{S} + \lambda_1 \left(\frac{d\boldsymbol{S}}{dt} - (\nabla \boldsymbol{V})^T \cdot \boldsymbol{S} - \boldsymbol{S} \cdot (\nabla \boldsymbol{V}) \right) = \mu_{nf}(\nabla \boldsymbol{V} + (\nabla \boldsymbol{V})^T), \tag{4}$$

where $\boldsymbol{V}$ is fluid velocity vector, ρ_{nf} is the density of the nanofluid, P is the pressure, $\boldsymbol{F}$ is the body force, $(\rho C)_{nf}$ is the heat capacity of the nanofluid, T is temperature, k_{nf} is the thermal conductivity of the nanofluid, $\boldsymbol{q}_r$ is the radiation heat flux vector, $\left(\frac{d}{dt}\right)$ denotes the material time derivative and ∇^2 is the Laplacian operator in the second order, $\boldsymbol{S}$ is the extra stress tensor for Maxwell fluid, λ_1 is the fluid relaxation time and μ_{nf} is the kinematic viscosity coefficient of the nanofluid, $\nabla \boldsymbol{V}$ is the velocity gradient and its transpose is $(\nabla \boldsymbol{V})^T$.

The right and left wall boundaries and the geometry of the surfaces (Gharsseldien *et al*. 2010) are defined by

$$Y = H_1 = d_1 + a_1 \sin\left[\frac{2\pi}{\lambda}(X - c\,t)\right], \tag{5}$$

$$Y = H_2 = -\,d_2 - \,b_1 \sin\left[\frac{2\pi}{\lambda}(X - c\,t) + \vartheta\right], \tag{6}$$

where λ is the wavelength, $(d_1 + d_2)$ is the width of the channel, ϑ is the phase difference that varies in the range $0 \le \vartheta \le \pi$, a_1 and b_1 are the amplitudes of the waves, where $a_1^2 + b_1^2 + 2a_1 b_1 \cos\vartheta \le (d_1 + d_2)^2$

Let (V, U) are components of the velocity in Y and X directions respectively. Considering $\boldsymbol{B} = (B_0, 0, 0)$ is the uniform magnetic field applied in the transverse direction to the flow, then the MHD force $\boldsymbol{J} \times \boldsymbol{B} = \left(0, -\sigma_{nf} B_0^2 U, 0\right)$, where $\boldsymbol{J}$ is the total current density, if there are no applied or polarized voltages and σ_{nf} is the electric conductivity. If $\boldsymbol{R}$ is Darcy's resistance for a fluid in a porous medium whereas in Maxwell fluid Darcy's resistance $\boldsymbol{R}$ (Gharsseldien and Awaad 2022), satisfies the relation $\left(1 + \lambda_1 \frac{d}{dt}\right)\boldsymbol{R} = -\frac{\mu_{nf}}{K}(V, U, 0)$, where K is the permeability

parameter.

Also, if $\boldsymbol{q}_r$ is the radiative heat flux, then according to Rosseland approximation for radiation (Mirzaei *et al.* 2023), $\boldsymbol{q}_r$ in $Y-$ direction will be $\boldsymbol{q}_r = \left(-\frac{4}{3}\frac{\sigma_0}{k_0}\frac{\partial T^4}{\partial Y},\ 0,\ 0\right)$, where σ_0 is Stefan-Boltzman constant and k_0 is the Rosseland mean absorption coefficient.

Moreover, we suppose that the temperature difference within the flow is sufficiently small such that T^4 may be expanded in a Taylor series. Hence, expanding T^4 about T_0 and ignoring higher-order terms we get $T^4 \cong 4\ T_0^3\ T - 3\ T_0^4$, i.e., $\boldsymbol{q}_r = \left(-\frac{16}{3}\frac{\sigma_0 T_0^3}{k_0}\frac{\partial T}{\partial Y}, 0, 0\right)$.

In the vertical channel the external force including a gravity force as a function of temperature acts on the vertical direction X. The gravity force is $\boldsymbol{g} = \left(0,\ g(\rho\alpha)_{nf}(T - T_0), 0\right)$

Then Eqs. (1)-(4) will be on the form

$$\frac{\partial U}{\partial X} + \frac{\partial V}{\partial Y} = 0, \tag{7}$$

$$\begin{aligned}&\rho_{nf}\left(1 + \lambda_1\frac{d}{dt}\right)\left(\frac{d\ U}{dt}\right)\\ &= \left(1 + \lambda_1\frac{d}{dt}\right)\left[-\ \frac{\partial P}{\partial X} + \frac{\partial S_{XX}}{\partial X} + \frac{\partial S_{XY}}{\partial Y} - \sigma_{nf}B_0^2 U\right]\\ &\quad + \left(1 + \lambda_1\frac{d}{dt}\right)\left[g\ (\rho\alpha)_{nf}(T - T_0)\right] - \frac{\mu_{nf}}{K}U,\end{aligned} \tag{8}$$

$$\begin{aligned}&\rho_{nf}\left(1 + \lambda_1\frac{d}{dt}\right)\left(\frac{dV}{dt}\right)\\ &= -\left(1 + \lambda_1\frac{d}{d\ t}\right)\ \left[\frac{\partial P}{\partial Y} + \frac{\partial S_{YX}}{\partial X} + \frac{\partial S_{YY}}{\partial Y}\right] - \frac{\mu_{nf}}{K}V,\end{aligned} \tag{9}$$

$$\begin{aligned}&(\rho C)_{nf}\left(\frac{dT}{dt}\right) = k_{nf}\left(\frac{\partial^2 T}{\partial X^2} + \frac{\partial^2 T}{\partial Y^2}\right) + S_{XX}\frac{\partial U}{\partial X}\\ &+ S_{XY}\frac{\partial U}{\partial Y} + S_{YX}\frac{\partial V}{\partial X} + S_{YY}\frac{\partial V}{\partial Y} + \frac{16}{3}\frac{\sigma_0 T_0^3}{k_0}\frac{\partial^2 T}{\partial Y^2},\end{aligned} \tag{10}$$

$$S_{XX} + \lambda_1\left[\frac{dS_{XX}}{dt} - 2\left(S_{XX}\frac{\partial U}{\partial X} + S_{XY}\frac{\partial U}{\partial Y}\right)\right] = 2\mu_{nf}\frac{\partial U}{\partial X}, \tag{11}$$

$$\begin{aligned}&S_{XY}\ or\ S_{YX} + \lambda_1\left[\frac{dS_{XY}}{dt} - S_{XX}\frac{\partial V}{\partial X} - S_{YY}\frac{\partial U}{\partial Y}\right]\\ &= \mu_{nf}\left(\frac{\partial V}{\partial X} + \frac{\partial U}{\partial Y}\right)\end{aligned} \tag{12}$$

$$S_{YY} + \lambda_1\left[\frac{dS_{YY}}{dt} - 2\left(S_{XY}\frac{\partial V}{\partial X} + S_{YY}\frac{\partial V}{\partial Y}\right)\right] = 2\mu_{nf}\frac{\partial V}{\partial Y}, \tag{13}$$

where g is the acceleration due to gravity and α_{nf} is the thermal expansion coefficient of nanofluid.

Using (y, x) as a wave frame moving with the velocity c away from (Y, X) the laboratory frame, by the transformations

$$\begin{aligned}&y = Y, \quad x = X - c\ t, \quad u = U - c,\\ &v = V, \quad p\ (x) = P(X, t),\end{aligned} \tag{14}$$

where p is the pressure of the fluid, v and u are the velocity components, in the wave frame of references. Also, introducing the non-dimensional variables

$$\left.\begin{aligned}&\bar{y} = \frac{y}{d_1}, \quad \bar{x} = \frac{x}{\lambda}, \quad \bar{t} = \frac{ct}{\lambda}, \quad \bar{u} = \frac{u}{c}, \quad \bar{v} = \frac{v}{\delta c},\\ &h_1 = \frac{H_1}{d_1}, \quad h_2 = \frac{H_2}{d_1}, \quad b = \frac{b_1}{d_1}, \quad a = \frac{a_1}{d_1}, \quad d = \frac{d_2}{d_1},\\ &\delta = \frac{d_1}{\lambda}, \quad \bar{\lambda}_1 = \lambda_1\frac{c}{d_1}, \quad p = \frac{d_1^2\bar{p}}{\mu_f c\,\lambda}, \quad \overline{R} = \frac{K}{d_1^2},\\ &\Theta = \frac{T - T_0}{T_1 - T_0}, \quad M = \sqrt{\frac{\sigma_f}{\mu_f}}B_0 d_1, \quad \overline{S} = \frac{d_1}{c\ \mu_f}S,\\ &G_r = \frac{g\ (\rho\alpha)_f\ d_1^2(T_1 - T_0)}{c\ \mu_f}, \quad R_e = \frac{\rho_f\ c\ d_1}{\mu_f}\\ &E_c = \frac{c^2}{C_f(T_1 - T_0)}, \quad P_r = \frac{\mu_f\ C_f}{k_f}, \quad R_n = \frac{16\ \sigma_0\ T_0^3}{3k_0\ k_f}\end{aligned}\right\} \tag{15}$$

where M is the Hartmann number, R_e is the Reynolds number, Θ is the dimensionless temperature, C_f is the specific heat of the fluid, μ_f is the kinematic viscosity coefficient of the fluid, G_r is Grashof numbers, $\frac{1}{R_n}$ is the Stark number (R_n is the conduction–radiation parameter), P_r is the Prandtl number and E_c is the Eckert number.

By using Eqs. (14) and (15), dropping bars, low Reynolds number, and under the long-wavelength assumptions ($\delta \ll 1$), Eqs. (7)-(13) become on the form

$$\begin{aligned}&\frac{\partial p}{\partial x} = \frac{\partial S_{xy}}{\partial y} - \left(\frac{\sigma_{nf}}{\sigma_f}M^2 + \frac{\mu_{nf}}{\mu_f}\frac{1}{K}\right)(u + 1)\\ &+ \frac{(\rho\alpha)_{nf}}{(\rho\alpha)_f}\ G_r\ \Theta,\end{aligned} \tag{16}$$

$$\frac{\partial p}{\partial y} = 0, \tag{17}$$

$$\frac{1}{P_r}\left(\frac{k_{nf}}{k_f} + R_n\right)\left(\frac{\partial^2\Theta}{\partial y^2}\right) + E_c\ S_{xy}\left(\frac{\partial u}{\partial y}\right) = 0, \tag{18}$$

$$S_{xx} - 2\lambda_1\ S_{xy}\frac{\partial u}{\partial y} = 0, \tag{19}$$

$$S_{xy}\ \text{ or }\ S_{yx} - \lambda_1\ S_{yy}\frac{\partial u}{\partial y} = \frac{\mu_{nf}}{\mu_f}\frac{\partial u}{\partial y}, \tag{20}$$

$$S_{yy} = 0, \tag{21}$$

Also, right and left channel walls in dimensionless forms will be

$$y = h_1 = 1 + a\ \sin 2\pi x \tag{22}$$

$$y = h_2 = -d - b\ (\sin 2\pi x + \vartheta) \tag{23}$$

After eliminating the pressure between Eqs. (16) and (17) and then using Eqs. (20) and (21), the equations of motion in terms of the stream function ψ $\left(\text{where } u = \frac{\partial\psi}{\partial y}, v = -\frac{\partial\psi}{\partial x}\right)$, will be

$$\psi_{yyyy} - N^2\psi_{yy} + G_r\frac{(\rho\alpha)^*}{\mu^*}\ \Theta_y = 0, \tag{24}$$

$$\Theta_{yy} + B_r\frac{\mu^*}{\chi^*}\left(\psi_{yy}\right)^2 = 0, \tag{25}$$

Table 1 The values of effective ratios of thermo-physical properties of some base fluids and nanoparticles

		Base Fluid (UCM)								
		Pure Water			Ethylene Glycol			Blood		
		$(\rho\alpha)_r$	k_r	σ_r	$(\rho\alpha)_r$	k_r	σ_r	$(\rho\alpha)_r$	k_r	σ_r
Nanoparticles	Copper (Cu)	0.7125	654	1.19E+09	0.2060	1591	5.57E+07	1.4074	740	8.51E+07
	Silver (Ag)	0.9478	700	1.26E+09	0.2740	1702	5.89E+07	1.8722	792	9.00E+07
	Gold (Au)	1.3088	519	9.04E+08	0.3785	1261	4.22E+07	2.5855	587	6.46E+07
	Alumina (Al_2O_3)	0.1612	65	3.00E-06	0.0466	159	1.40E-07	0.3183	74	2.14E-07
	Titanium Oxide (TiO_2)	0.1827	15	2.00E-11	0.0528	36	0.35E-13	0.3608	17	1.43E-12

where $N^2 = \left(\frac{\sigma^*}{\mu^*}M^2 + \frac{1}{K}\right)$, $\chi^* = (k^* + R_n)$, $P_r E_c = B_r$ is the Brinkman number, the dynamic viscosity of nanofluids according to (Sheikholeslami *et al*. 2012) is

$$\mu^* = \frac{\mu_{nf}}{\mu_f} = \frac{1}{(1-\phi)^{2.5}} \tag{26}$$

the relation of effective density and thermal expansion coefficient of the nanofluid is

$$(\rho\alpha)^* = \frac{(\rho\alpha)_{nf}}{(\rho\alpha)_f} = 1 + \phi\ [(\rho\alpha)_r - 1] \tag{27}$$

the effective thermal conductivity of the nanofluid according to Hamilton (1962) is

$$k^* = \frac{k_{nf}}{k_f} = 1 + \frac{\phi\, m\, [k_r - 1]}{m + (1-\phi)[k_r - 1]} \tag{28}$$

the effective electrical conductivity of nanofluid was presented by (Sheikholeslami *et al*. 2014) as

$$\sigma^* = \frac{\sigma_{nf}}{\sigma_f} = 1 + \frac{3\phi[\sigma_r - 1]}{3 + (1-\phi)\,[\sigma_r - 1]} \tag{29}$$

with $(\rho\alpha)_r = \frac{(\rho\alpha)_p}{(\rho\alpha)_f}$, $k_r = \frac{k_p}{k_f}$, $\sigma_r = \frac{\sigma_p}{\sigma_f}$, where $(.)_p$ is the physical property of nanoparticles $(.)_r$ is the ratio of the same property, ϕ is the nanoparticle volume fraction ($\phi = 0.05$ through the paper), and m is the shape factor, ($m = \frac{3}{\xi}$ where ξ is the sphericity which is used to characterize the shape of particles falling through fluids). In the resultant system of Eqs. (22)-(29), when $\vartheta = 0$, $d = 1$, $b = a$ and $R_n = 0$ we get (Gharsseldien and Awaad 2022) as a special case.

The values of thermo-physical properties of some base fluids and nanoparticles at temperature 300 K are presented by Sheikholeslami and Ganji (2017), Sobamowo (2018) and Turns and Kraige (2007). Table 1 presented by Gharsseldien and Awaad (2022) which refers to the calculated values of effective ratios of thermophysical properties of some base fluids and nanoparticles.

In terms of the stream function, the appropriate dimensionless boundary conditions are

$$\begin{aligned} &\psi = \tfrac{q}{2}, \quad \psi_y = -1, \quad \Theta = 0, \\ &at \quad y = h_1 = 1 + a\,\sin 2\pi x \end{aligned} \tag{30}$$

$$\begin{aligned} &\psi = -\frac{q}{2}, \quad \psi_y = -1, \quad \Theta = 1, \\ &at \quad y = h_2 = -d - b\ (\sin 2\pi x + \vartheta), \end{aligned} \tag{31}$$

where q represents fluid flow rate in wave frame and will discuss in detail in pumping characteristics.

3. The solution to the problem

The governing differential Eqs. (24)-(25) with boundary conditions in Eqs. (30)-(31) consists of non-linear and coupled equations. Getting the exact solution of the governing system of equations is difficult and unavailable. The perturbation method gives an analytical solution understanding of the behavior of some phenomena in life problems and is close to the exact solution without discretization or linearization and it is more insightful than purely numerical methods. Therefore, using the perturbation method may give an analytical solution to the system. By taking Brinkman number B_r as a perturbation parameter, we expand the functions $\psi(x,y)$ and $\Theta(x,y)$ as follows

$$\psi(y,x) = \psi_0(y,x) + B_r\ \psi_1(y,x) + B_r^2\ \psi_2(y,x) + \ldots$$
$$\Theta(y,x) = \Theta_0(y,x) + B_r\ \Theta_1(y,x) + B_r^2\ \Theta_2(y,x) + \ldots$$

Substituting into the differential Eqs. (24)-(25), and boundary conditions in Eqs. (30)-(31), we have

3.1 Zero order

$$(\psi_0)_{yyyy} - N^2(\psi_0)_{yy} + G_r\frac{(\rho\alpha)^*}{\mu^*}\ (\Theta_0)_y = 0 \tag{32}$$

$$(\Theta_0)_{yy} = 0 \tag{33}$$

$$\begin{aligned} &\psi_0 = \frac{q}{2}, \quad (\psi_0)_y = -1, \quad \Theta_0 = 0, \\ &at \quad y = h_1 = 1 + a\ \sin\ 2\pi x \end{aligned} \tag{34}$$

$$\begin{aligned} &\psi_0 = -\frac{q}{2}, \quad (\psi_0)_y = -1, \quad \Theta_0 = 1, \\ &at \quad y = h_2 = -d - b\ (\sin 2\pi x + \vartheta) \end{aligned} \tag{35}$$

The exact solution of zero order stream and heat functions are given as

$$\psi_0(y,x) = -\left(\frac{2y - h_1 - h_2}{2}\right) + (q + h_1 - h_2)\begin{bmatrix} \sinh\left[N\left(\frac{2y-h_1-h_2}{2}\right)\right] \\ \hline 2\sinh\left[N\left(\frac{h_1-h_2}{2}\right)\right] \\ -N\left(\frac{2y-h_1-h_2}{2}\right)\cosh\left[N\left(\frac{h_1-h_2}{2}\right)\right] \\ -(h_1-h_2)N\cosh\left[N\left(\frac{h_1-h_2}{2}\right)\right] \end{bmatrix} \tag{36}$$

$$+G_r\frac{(\rho\alpha)^*}{\mu^*}\left[\frac{(y-h_2)(h_1-y)}{2N^2(h_1-h_2)}+\frac{\cosh\left[N\left(\frac{2y-h_1-h_2}{2}\right)\right]-\cosh\left[N\left(\frac{h_1-h_2}{2}\right)\right]}{2N^3\sinh\left[N\left(\frac{h_1-h_2}{2}\right)\right]}\right]$$

$$\Theta_0(y,x)=\frac{h_1-y}{h_1-h_2} \tag{37}$$

3.2 First order

$$(\psi_1)_{yyyy}-N^2(\psi_1)_{yy}+G_r\frac{(\rho\alpha)^*}{\mu^*}\ (\Theta_1)_y=0, \tag{38}$$

$$(\Theta_1)_{yy}+\frac{\mu^*}{\chi^*}\left((\psi_0)_{yy}\right)^2=0, \tag{39}$$

$$\begin{aligned}&\psi_1=0,\qquad (\psi_1)_y=0,\quad \Theta_1=0,\\ &at\quad y=h_1=1+a\ \sin 2\pi x,\end{aligned} \tag{40}$$

$$\begin{aligned}&\psi_1=0,\ \ (\psi_1)_y=0,\quad \Theta_1=0,\\ &at\quad y=h_2=-d-b\ \ (\sin 2\pi x+\vartheta),\end{aligned} \tag{41}$$

$$\begin{aligned}\psi_1(x,y)&=L_1+L_2\left(\frac{2y-h_1-h_2}{2}\right)\\ &+L_3\sinh\left[N\left(\frac{2y-h_1-h_2}{2}\right)\right]+L_4\cosh\left[N\left(\frac{2y-h_1-h_2}{2}\right)\right]\\ &+G_r\frac{(\rho\alpha)^*}{6\mu^*N^3}\begin{pmatrix}C_4\sinh[N(2y-(h_1+h_2))]\\ +C_3\cosh[N(2y-(h_1+h_2))]\\ +3C_1\left[N\left(y-\frac{h_1+h_2}{2}\right)\right]\sinh\left[N\left(\frac{2y-h_1-h_2}{2}\right)\right]\\ +3C_2\left[N\left(\frac{2y-h_1-h_2}{2}\right)\right]\cosh\left[N\left(\frac{2y-h_1-h_2}{2}\right)\right]\\ +(y-h_2)(h_1-y)\ (N(2y-(h_1+h_2))C_5-3NC_6)\end{pmatrix}\end{aligned} \tag{42}$$

$$\begin{aligned}\Theta_1(x,y)&=-C_1\sinh\left[N\left(\frac{2y-h_1-h_2}{2}\right)\right]\\ &-C_2\cosh\left[N\left(\frac{2y-h_1-h_2}{2}\right)\right]\\ &-C_3\sinh[N(2y-(h_1+h_2))]\\ &-C_4\cosh[N(2y-(h_1+h_2))]\\ &-C_5\left(\frac{2y-h_1-h_2}{2}\right)^2+C_6\left(\frac{2y-h_1-h_2}{2}\right)+C_7\end{aligned} \tag{43}$$

where

$$C_1=G_r\frac{(\rho\alpha)^*}{2(k^*+R_n)N^2\left(\frac{h_1-h_2}{2}\right)}\left[\frac{q+(h_1-h_2)}{N\left(\frac{h_1-h_2}{2}\right)\cosh\left[N\left(\frac{h_1-h_2}{2}\right)\right]-\sinh\left[N\left(\frac{h_1-h_2}{2}\right)\right]}\right]$$

$$C_2=-G_r^2\frac{(\rho\alpha)^{*2}}{2\mu^*(k^*+R_n)N^5\left(\frac{h_1-h_2}{2}\right)}\left[\frac{1}{\sinh\left[N\left(\frac{h_1-h_2}{2}\right)\right]}\right],$$

$$C_3=-G_r\frac{(\rho\alpha)^*}{8(k^*+R_n)N}\left[\frac{(q+(h_1-h_2))}{1-\cosh[N(h_1-h_2)]+\left[N\left(\frac{h_1-h_2}{2}\right)\right]\sinh[N(h_1-h_2)]}\right],$$

$$C_4=\frac{C_3}{2}\left[\frac{C_2}{C_1}+\frac{C_1}{C_2}\right],\qquad C_5=N^2\left[\frac{C_2C_3}{C_1}-\frac{C_1C_3}{C_2}+\frac{C_1C_2}{32C_3}\right],$$

$$C_6=\frac{2}{h_1-h_2}\left[C_1\sinh\left[N\left(\frac{h_1-h_2}{2}\right)\right]+C_3\sinh[N(h_1-h_2)]\right],$$

$$C_7=C_2\cosh\left[N\left(\frac{h_1-h_2}{2}\right)\right]+C_4\cosh[N(h_1-h_2)]+C_5\left(\frac{h_1-h_2}{2}\right)^2$$

$$L_1=G_r\frac{(\rho\alpha)^*}{4\mu^*N^3}\left[C_3+\frac{\begin{pmatrix}3[N(h_1-h_2)]C_1\\ +6(h_1-h_2)C_6\cosh\left[N\left(\frac{h_1-h_2}{2}\right)\right]\\ +3C_1\sinh[N(h_1-h_2)]\\ +C_3\sinh\left[3N\left(\frac{h_1-h_2}{2}\right)\right]\end{pmatrix}}{3\sinh\left[N\left(\frac{h_1-h_2}{2}\right)\right]}\right]$$

$$L_2=G_r\frac{(\rho\alpha)^*}{12\mu^*N^2}\left[\frac{\begin{pmatrix}-3[N(h_1-h_2)]C_2\\ -\left(3C_4+8C_5\left(\frac{h_1-h_2}{2}\right)^2\right)\sinh\left[N\left(\frac{h_1-h_2}{2}\right)\right]\\ +3C_2\sinh[N(h_1-h_2)]\\ +C_4\sinh\left[3N\left(\frac{h_1-h_2}{2}\right)\right]\end{pmatrix}}{N\left(\frac{h_1-h_2}{2}\right)\cosh\left[N\left(\frac{h_1-h_2}{2}\right)\right]-\sinh\left[N\left(\frac{h_1-h_2}{2}\right)\right]}\right]$$

$$L_3=G_r\frac{(\rho\alpha)^*}{6\mu^*N^3}\left[\frac{\begin{pmatrix}4N\left(\frac{h_1-h_2}{2}\right)^3C_5\\ -3N^2\left(\frac{h_1-h_2}{2}\right)^2C_2\sinh\left[N\left(\frac{h_1-h_2}{2}\right)\right]\\ +C_4\sinh[N(h_1-h_2)]\\ -[N(h_1-h_2)]C_4\cosh[N(h_1-h_2)]\end{pmatrix}}{N\left(\frac{h_1-h_2}{2}\right)\cosh\left[N\left(\frac{h_1-h_2}{2}\right)\right]-\sinh\left[N\left(\frac{h_1-h_2}{2}\right)\right]}\right]$$

$$L_4=-G_r\frac{(\rho\alpha)^*}{6\mu^*N^3}\left[3C_1+\frac{\begin{pmatrix}3(h_1-h_2)C_6\\ +3\left[N\left(\frac{h_1-h_2}{2}\right)\right]C_1\cosh\left[N\left(\frac{h_1-h_2}{2}\right)\right]\\ +2C_3\sinh[N(h_1-h_2)]\end{pmatrix}}{\sinh\left[N\left(\frac{h_1-h_2}{2}\right)\right]}\right]$$

In zero order solution represented by Eqs. (36)-(37) and first order solution represented by Eqs. (42)-(43) when $\vartheta=0$, $d=1$, $b=a$ and $R_n=0$ we get (Gharseldien and Awaad 2022) as a special case.

4. Pumping characteristics

The fluid flow rate in the wave frame can be expressed as: $q=\int_{h_2}^{h_1}u(y,x)dy$

While the fluid flow rate in the laboratory frame can be written as $Q=\int_{H_2}^{H_1}U(y,x,t)dY$

From the equations that were used to convert from the laboratory frame to the wave frame, $X=x+t$, and $U=$

$u+1$ we can conclude the following relationship $Q = q + h_1 - h_2$

Supposing we are dealing with a device of a pumping nature, accordingly, it is good to find a discharge rate $\bar{Q}$, which can be used as the meantime of the volumetric flow rate for each cross-section as $\bar{Q} = q + 1 + \mathrm{d}$

The pressure gradient and the pressure rise are important to study peristaltic transport. In accordance with the perturbation technique used, the pressure gradient is represented as

$$\frac{dp(x)}{dx} = \frac{dp_0(x)}{dx} + B_r \frac{dp_1(x)}{dx} + \cdots \tag{44}$$

where

$$\frac{dp_0(x)}{dx} = \frac{(\rho\alpha)^* G_r}{2} - \frac{\mu^* N^3 (q + \mathrm{h}_1 - \mathrm{h}_2)\cosh\left(N\left(\frac{h_1-h_2}{2}\right)\right)}{N(h_1-h_2)\cosh\left(N\left(\frac{h_1-h_2}{2}\right)\right) - 2\sinh\left(N\left(\frac{h_1-h_2}{2}\right)\right)},$$

$$\frac{dp_1(x)}{dx} = (\rho\alpha)^* G_r C_7 - \mu^* N^2 L_2 - \frac{(\rho\alpha)^* G_r \left(6 - N^2\left(\frac{h_1-h_2}{2}\right)^2\right)}{3N^2} C_5$$

Integrating Eq. (44) over one wavelength λ, the pressure rise will $\Delta p = \int_0^1 \frac{dp}{dx}\, dx = \int_0^1 \left(\frac{dp_0}{dx} + B_r \frac{dp_1}{dx} + \cdots\right) dx = \Delta p_0 + B_r \Delta p_1 + \cdots$

where

$$\Delta p_0 = \frac{(\rho\alpha)^* G_r}{2} - \int_0^1 \frac{\mu^* N^3 (\bar{Q} - 1 - d + \mathrm{h}_1 - \mathrm{h}_2)\cosh\left(N\left(\frac{h_1-h_2}{2}\right)\right)}{N(h_1-h_2)\cosh\left(N\left(\frac{h_1-h_2}{2}\right)\right) - 2\sinh\left(N\left(\frac{h_1-h_2}{2}\right)\right)} dx,$$

$$\Delta p_1 = \int_0^1 \left((\rho\alpha)^* G_r C_7 - \mu^* N^2 L_2 - \frac{(\rho\alpha)^* G_r \left(6 - N^2\left(\frac{h_1-h_2}{2}\right)^2\right)}{3N^2} C_5 \right) dx$$

5. Results and discussion

In this section, we investigated the combined effects of thermal radiation parameter R_n with some other parameters like (Nanoparticle shape parameter ξ, Grashof number G_r, Magnetic parameter M, and the volume flow rate parameter $\bar{Q}$) on the pressure rise ΔP, pressure gradient $\partial P/\partial x$ and vertical velocity component u. Also, the effects of asymmetric amplitude fraction ν and phase angle θ on the pressure rise ΔP, pressure gradient $\partial P/\partial x$, heat function distribution Θ and trapping phenomenon.

5.1 Pumping performance and pressure gradient

Figs. 2(a)-(c) show that the combined effects of R_n with each of (ξ, G_r and M) on the pressure rise ΔP. The pressure rise is considered an indicator of the type of pumping, the peristaltic pumping region ($\Delta P > 0$) and at free pumping ($\Delta P = 0$), and the augmented peristaltic pumping region ($\Delta P < 0$). The effects of ν and θ are displayed in Figs. 3-4. As shown in Fig. 2(a), the effect of

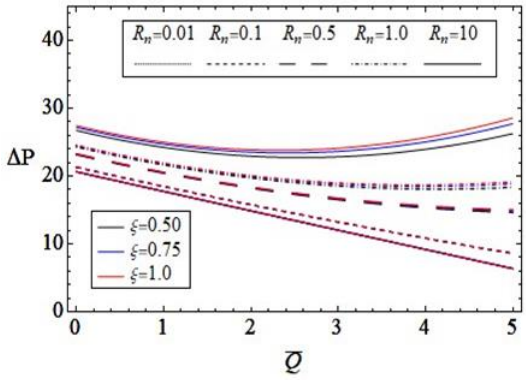

(a) Thermal radiation parameter (R_n) and the particle shape parameter (ξ) , $G_r = 4$, and $M = 0$

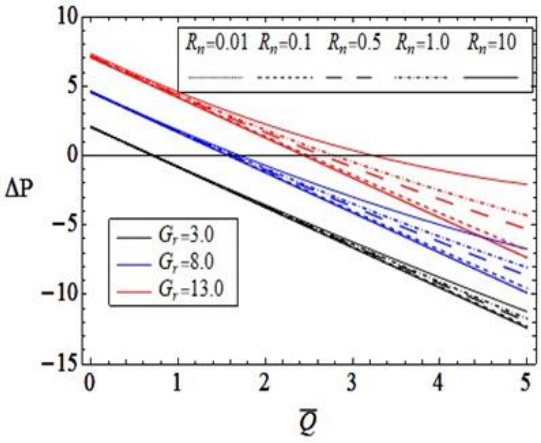

(b) Thermal radiation parameter (R_n) and Grash of number (G_r), $\xi = 1.0$, and $M = 0$

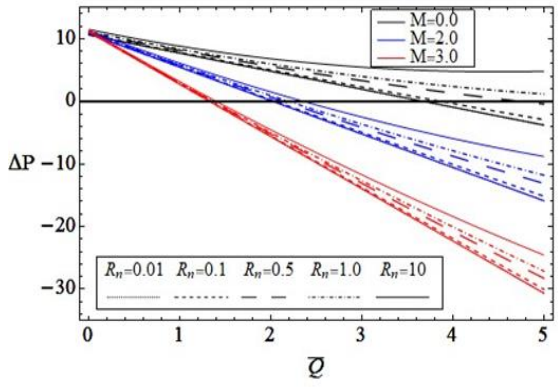

(c) Thermal radiation parameter (R_n) and Magnetic parameter (M), $\xi = 1.0$, $G_r = 20$

Fig. 2 Combined effects on pressure rise with $B_r = 0.1$, $\sigma_r = 1$, $k_r = 100$, $(\rho\alpha)_r = 1$, $K = 1$, $\nu = 1$ and $\theta = \frac{\pi}{2}$

variation in the geometric shape of the nanoparticles ξ appears when R_n is relatively large, and the pumping performance improves as the shape of the nanoparticle is more spherical. In Fig. 2(b), it is shown whether the effect of thermal radiation R_n is more evident in the case of large G_r, which means that the buoyancy force works to show this effect, and this combined effect indicates that the pumping performance improves when the buoyancy forces and thermal radiation are increase together. With constant

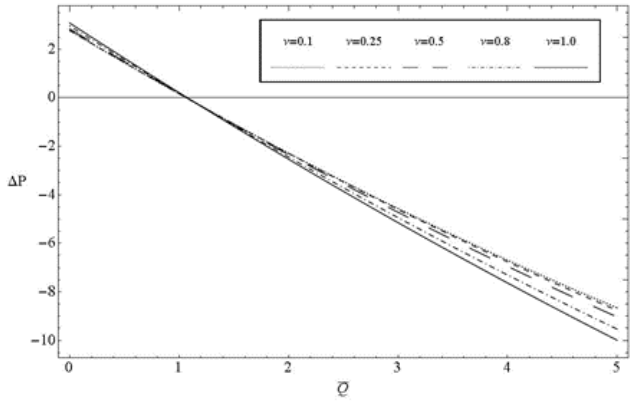

Fig. 3 Effect of asymmetric amplitude fraction (ν) on pressure rise with $\xi = 1.0, B_r = 0.1, \sigma_r = 1, k_r = 100, (\rho\alpha)_r = 1, M = 0, K = 1, R_n = 1, \theta = \frac{\pi}{2}$, and $G_r = 5$

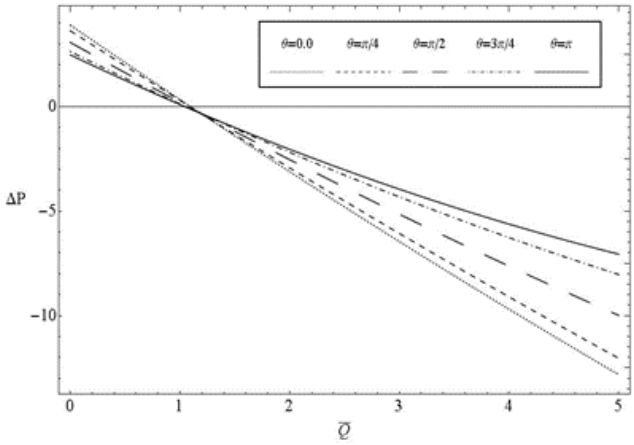

Fig. 4 Effect of phase angle (θ) on pressure rise wit $\xi = 1.0,\ B_r = 0.1, \sigma_r = 1, k_r = 100, (\rho\alpha)_r = 1,\ M = 0, K = 1, R_n = 1, \nu = 1,$ and $G_r = 5$

M, the effect of the variation of R_n appears, and the pumping performance improves as it increases. But with increasing the value of M, the effect of R_n follows the same behavior with lower values. Therefore, Fig. 2(c) indicates that the combined effect of thermal radiation and magnetism works to improve pumping performance by increasing R_n and decreasing M.

In Fig. 3 we clarified the effect of asymmetric amplitude fraction ν on pressure rise ΔP. There are two regions; one when $\Delta P > 0$ in this region ΔP increases with ν, and the second region when $\Delta P < 0$ we observed that ΔP decreases with ν, at $\Delta P = 0$ there is no effect of ν. There is no effect of θ on ΔP at $(\bar{Q} \cong 1.25)$ before it ΔP decreases with θ and after that point ΔP increases with θ as shown in Fig. 4.

In Fig. 5(a) we observe that, with increasing thermal radiation, the pressure gradient curves of the nanofluid with sphere-shaped nanoparticles are more potent than the other shapes. The impact of thermal conductivity as a function of the nanoparticle shape parameter is a way to clarify this

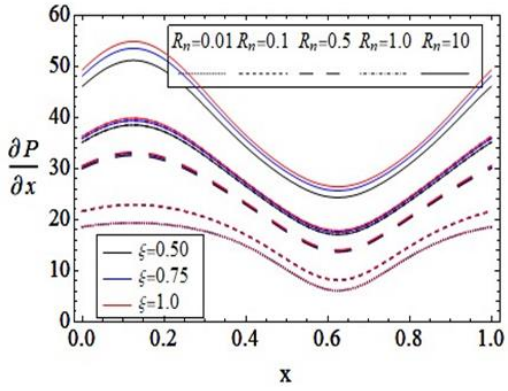

(a) Thermal radiation parameter (R_n) and the particle shape parameter (ξ), $M = 0$, $\bar{Q} = 4$, and $G_r = 50$

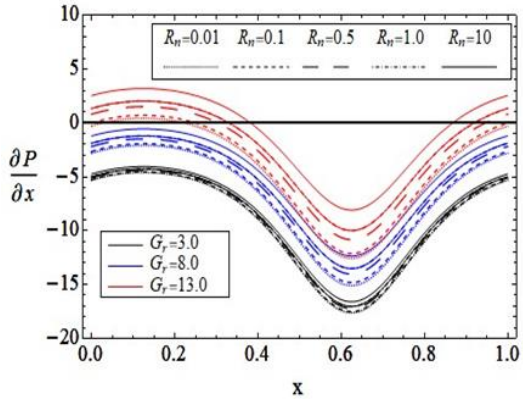

(b) Thermal radiation parameter (R_n) and Grashof number (G_r), $\xi = 1.0, \bar{Q} = 4,$ and $M = 0$

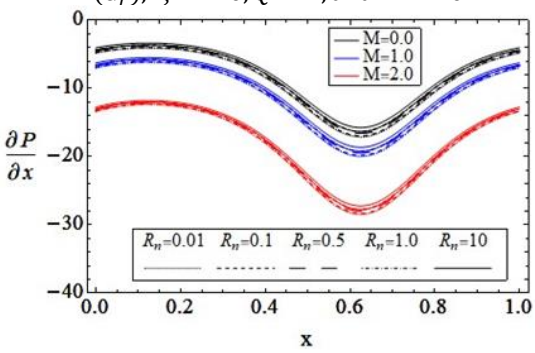

(c) Thermal radiation parameter (R_n) and Magnetic parameter (M), $\xi = 1.0$, $\bar{Q} = 4$, and $G_r = 4$

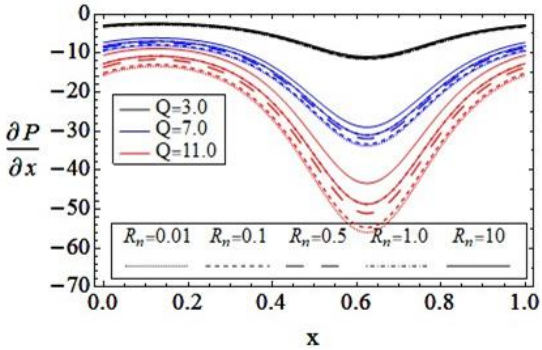

(d) Thermal radiation parameter (R_n) and the volume flow rate parameter $(\bar{Q}), \xi = 1.0,\ M = 0,$ and $G_r = 4$

Fig. 5 Combined effects on pressure gradient with $B_r = 0.1,\ \sigma_r = 1,\ k_r = 100,\ (\rho\alpha)_r = 1,\ K = 1, \nu = 1$ and $\theta = \frac{\pi}{2}$

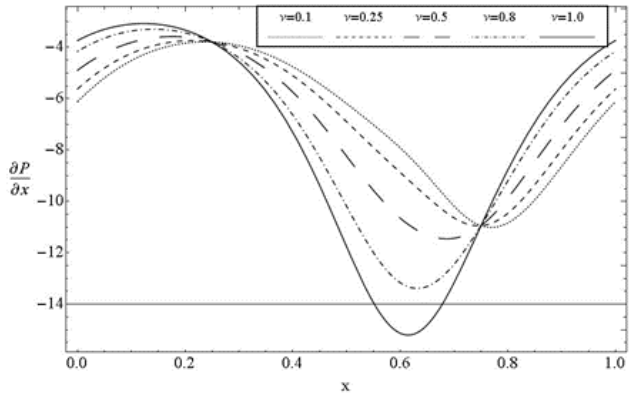

Fig. 6 Effect of asymmetric amplitude fraction (ν) on pressure gradient with $\xi = 1.0, B_r = 0.1, \sigma_r = 1, k_r = 100, (\rho\alpha)_r = 1, M = 0, K = 1, \bar{Q} = 4, R_n = 1, \theta = \frac{\pi}{2}$, and $G_r = 5$

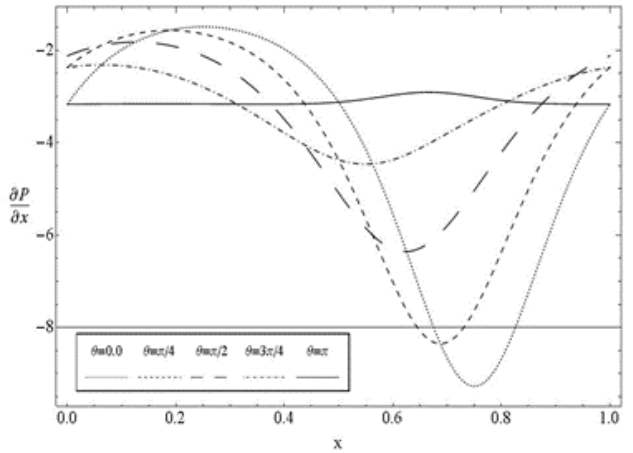

Fig. 7 Effect of phase angle (θ) on pressure gradient with $\xi = 1.0,\ B_r = 0.1,\ \sigma_r = 1,\ k_r = 100,\ (\rho\alpha)_r = 1,$ $M = 0, K = 1, \bar{Q} = 2, \nu = 1, R_n = 1,$ and $G_r = 3.0$

phenomenon. Whereas in Fig. 5(b) the same behavior presented by the variation of R_n with different values of M.

The effect of increasing G_r on the pressure gradient resulting from the change in the values of R_n is shown in Fig. 5(c), which shows that the values of G_r increase, the change becomes more obvious. The combined effect of thermal radiation and the volume flow rate $\bar{Q}$ is presented in Fig. 5(d) and it appears that the change is more clear with the increase of $\bar{Q}$, while the pressure gradient takes its lowest values when $\bar{Q}$ is increased and R_n is decreased together.

In Fig. 6 we studied the effect of ν on $\frac{\partial P}{\partial x}$, it is observed that the coordinates $x = 0.25$ and 0.75 are divided the frame into three regions; in first and last regions $\frac{\partial P}{\partial x}$ increased with ν and in the middle region $\frac{\partial P}{\partial x}$ decreased with ν it is obvious that for each value of ν any curve begins and ends at the same value of $\frac{\partial P}{\partial x}$ through the interval $0 \le x \le 1$.

Fig. 7 shows the effect of θ on $\frac{\partial P}{\partial x}$, where θ is one of the wall's parameters, (for each value of θ there is a different wall equation). We noticed that for each value of θ, the function has a behavior according to the value of θ, and $\frac{\partial P}{\partial x}$ has maximum and minimum values different for each θ, but at $\theta = \pi$ the pressure gradient has a constant value for all values of x.

5.2 The velocity

In Figs. 8(a)-(d), the effect of changing R_n with other variables appears on the vertical velocity component, and we notice that increasing R_n increases the velocity in the middle of the channel and decreases the velocity close to the walls, and the effect varies according to the temperature of the wall, as evidenced by the figures. There is no remarkable effect of varying nanoparticle shape parameter ξ with R_n as shown in Fig. 8(a). The combined effect of magnetic parameter M and thermal radiation parameter is displayed in Fig. 8(b), for low values of magnetic parameter M the change in velocity profile with R_n is apparent but for a large value of M the change has approximately disappeared.

5.3 Heat distibution

Figs. 9(a)-(d) explain the combined effect of radiation parameter R_n and each of the nanoparticle shape parameter ξ, magnetic parameter M, volumetric flow rate $\bar{Q}$, and Grashof number G_r on the heat function Θ (at $x = \frac{3}{4}$). In Fig. 9(a) the effect of nanoparticle shape is clearly at high radiation parameter and spherical nanoparticles increase the heat distribution more than the other shapes and this may be referred to the thermal conductivity which depends on the nanoparticle shape parameter ξ. While the greater the magnetic parameter M, the less the variation in the effect of increasing the thermal radiation parameter R_n, although it takes the same behavior as shown in Fig. 9(b).

Note that the effect of the porosity parameter K is the exact opposite of the effect of the magnetic parameter. The high values of the volume flow rate $\bar{Q}$ enlarge the effect of radiation parameter $R_n$on the heat function as displayed in Fig. 9(c). Although the heat function increases with the increase of radiation parameter, this effect shows slight variation with the change of Grashof number G_r as shown in Fig. 9(d). No remarkable effects for the amplitude ratio parameter ν, and the phase angle θ.

5.4 Trapping

In Figs. 10 and 11 we plotted the contours of the stream function versus its local position (y, x) with ν and θ. In Fig. 10(a) the right and left bolus are similar when $\nu = 1.0$, after that as ν decreased the left wall becomes more convex till be straight at very small values of ν and the concavity of the right bolus less but vice versa happened for

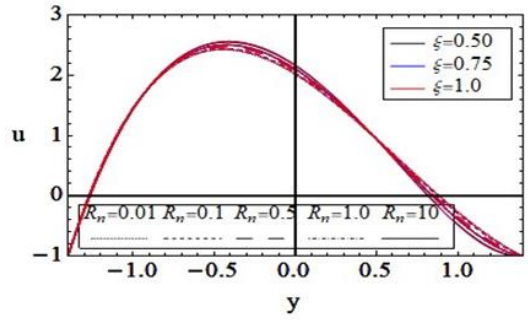

(a) Thermal radiation parameter (R_n) and particle shape parameter (ξ), $M = 0, \bar{Q} = 5,$ and $G_r = 20$

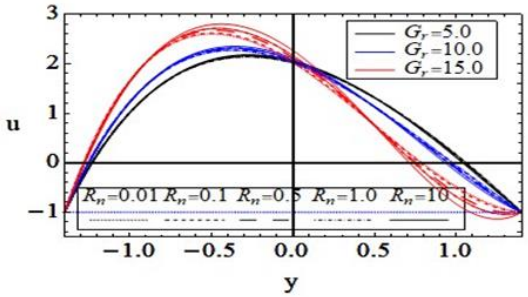

(b) Thermal radiation parameter (R_n) and Grashof number (G_r), $\xi = 1.0,$ $\bar{Q} = 5,$ and $M = 0$

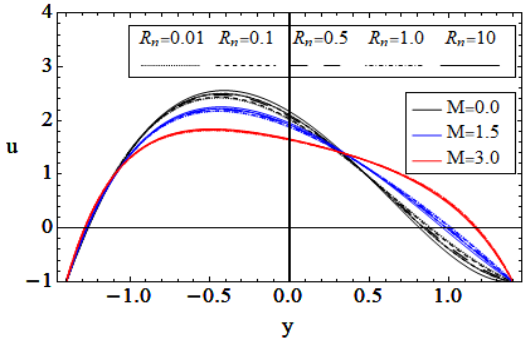

(c) Thermal radiation parameter (R_n) and Magnetic parameter (M), $\xi = 1.0, \bar{Q} = 5$, and $G_r = 20$

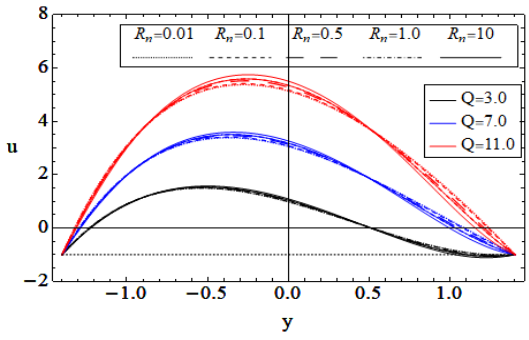

(d) Thermal radiation parameter (R_n) and the volume flow rate $(\bar{Q})$, $\xi = 1.0,$ $M = 0,$ and $G_r = 20$

Fig. 8 Combined effects on vertical velocity component with $B_r = 0.1,$ $\sigma_r = 1,$ $k_r = 100, (\rho\alpha)_r = 1, K = 1, \nu = 1$ and $\theta = 0$

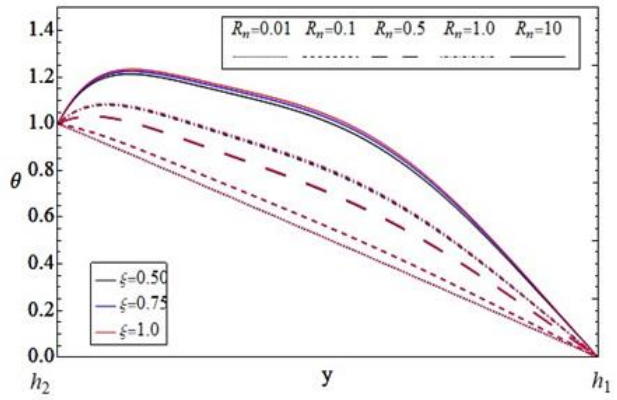

(a) Thermal radiation parameter (R_n) and particle shape parameter$(\xi), M = 0,$ $\bar{Q} = 4,$ $G_r = 30,$ and $\theta = 0$

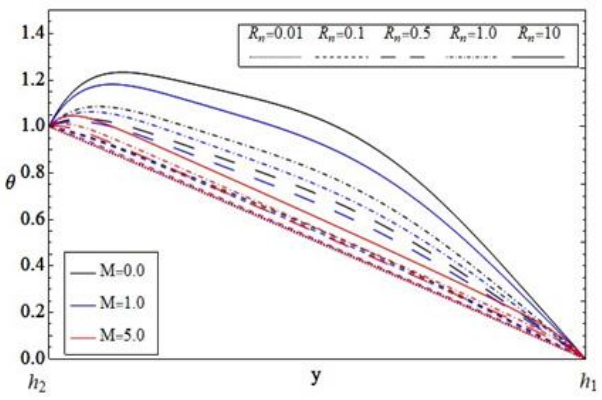

(b) Thermal radiation parameter (R_n) and Magnetic parameter (M), $\xi = 1.0, \bar{Q} = 4$, and $G_r = 30$

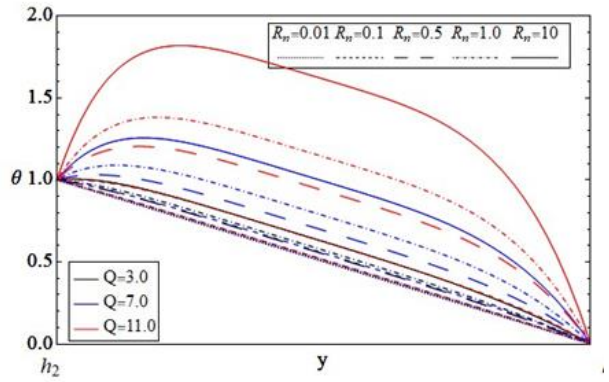

(c) Thermal radiation parameter (R_n) and volume flow rate $(\bar{Q})$, $\xi = 1.0,$ $M = 0,$ and $G_r = 5$

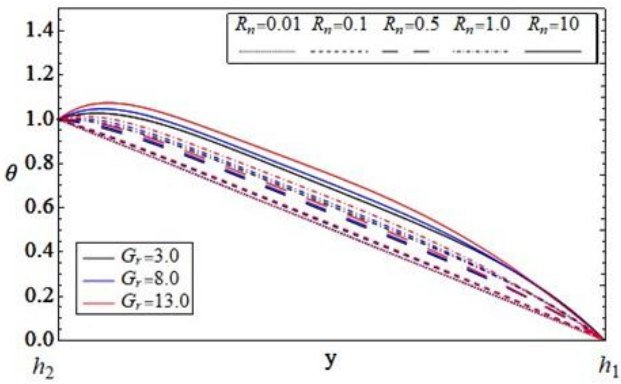

(d) Thermal radiation parameter (R_n) and Grashof number (G_r), $\xi = 1.0,$ $\bar{Q} = 4,$ and $M = 0$

Fig. 9 Combined effects on heat function with $B_r = 0.1, \sigma_r = 1,$ $k_r = 10, (\rho\alpha)_r = 1, K = 1, \nu = 1$ and $\theta = 0$

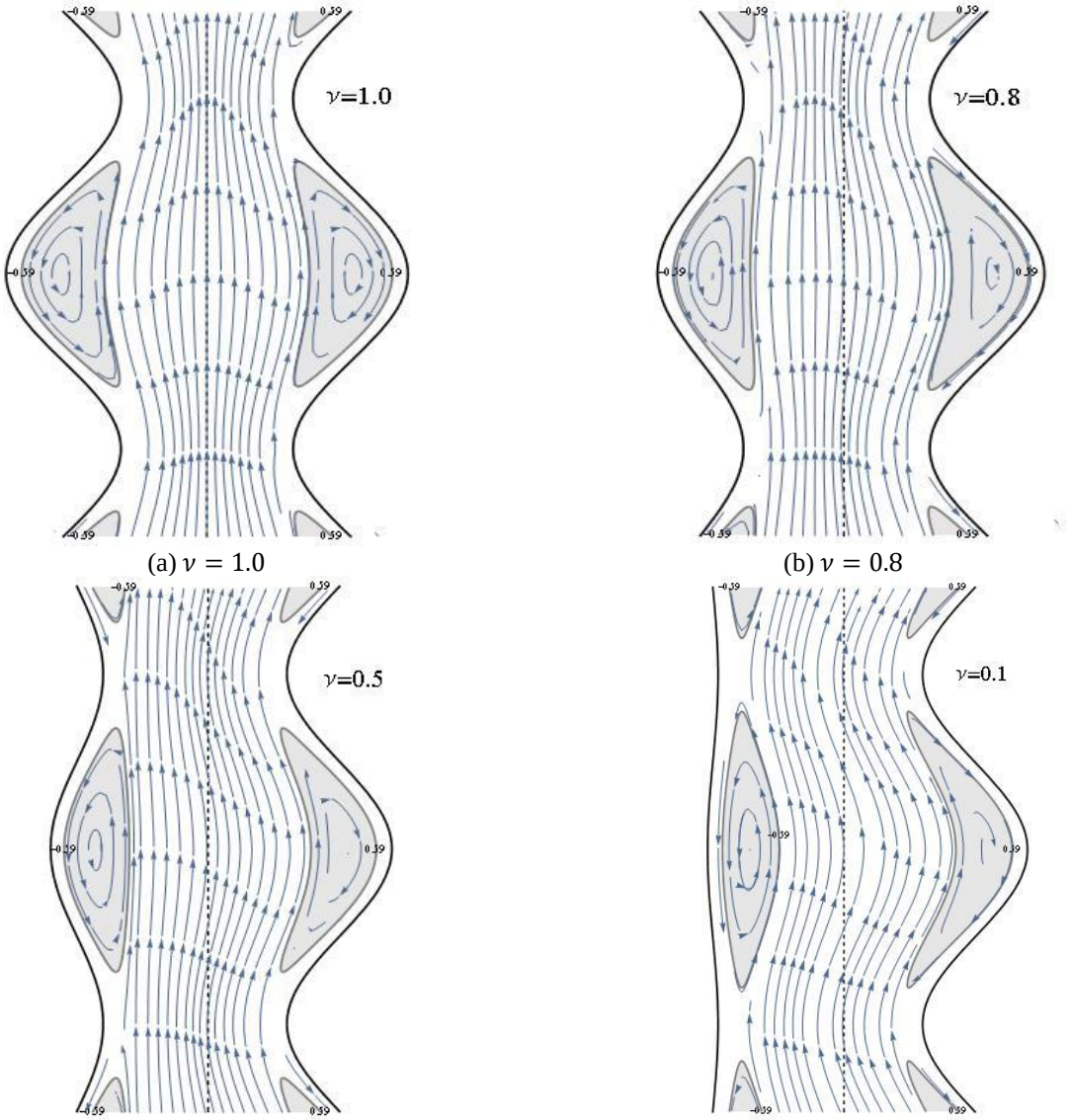

(a) $\nu = 1.0$ (b) $\nu = 0.8$

(c) $\nu = 0.5$ (d) $\nu = 0.1$

Fig. 10 Effect of amplitude fraction ν in trapping phenomena with $\xi = 1.0, B_r = 0.1, \sigma_r = 1, k_r = 100$, $(\rho\alpha)_r = 1, M = 0, R_n = 1.0, K = 1, \bar{Q} = 3, \theta = 0,$ and $G_r = 0$

the right bolus and the hump becomes faster as shown in Figs. 10(b)-(d). Fig. 11 we see that by increasing θ the two boluses are elongated until at $\theta = \pi$ the two boluses disappear, this confirms what we discussed in Fig. 7 when $\theta = \pi$.

6. Conclusions

The study presents how nanofluid flows in the presence of a magnetic field and a porous medium in a vertical channel with an asymmetrical peristaltic channel under the influence of thermal radiation. When the thermal radiation parameter changes in combination with some physical variables, there is a change in fluid behavior. The authors used a system of differential equations that describe the flow of a Maxwell nanofluid and the influences of magnetism, a porous medium, and thermal radiation. They obtained approximate solutions for the stream function and temperature function that describe the nanofluid behavior through these equations. In addition, the authors also found some parameters that describe the behavior of the fluid during its interaction with the vertical position, thermal radiation, the shape of the nanoparticle, and the magnetic field. The results of changing the parameters in this study are derived from the approximate solution using the perturbation method, and qualitatively, the summary of the results is as follows:

• At large values of both Grashof number G_r and radiation parameter R_n the effect of nanoparticle shape ξ appears in a pressure rise and pressure gradient.

• The appearance of reverse velocity happened at a large value of the radiation parameter R_n and (large value of Grashof number G_r, or small value of volume flow rate $\bar{Q}$).

• The pressure gradient has a constant value, at $\theta = \pi$ for all values of x.

• The nanoparticle shape effect appears at high radiation

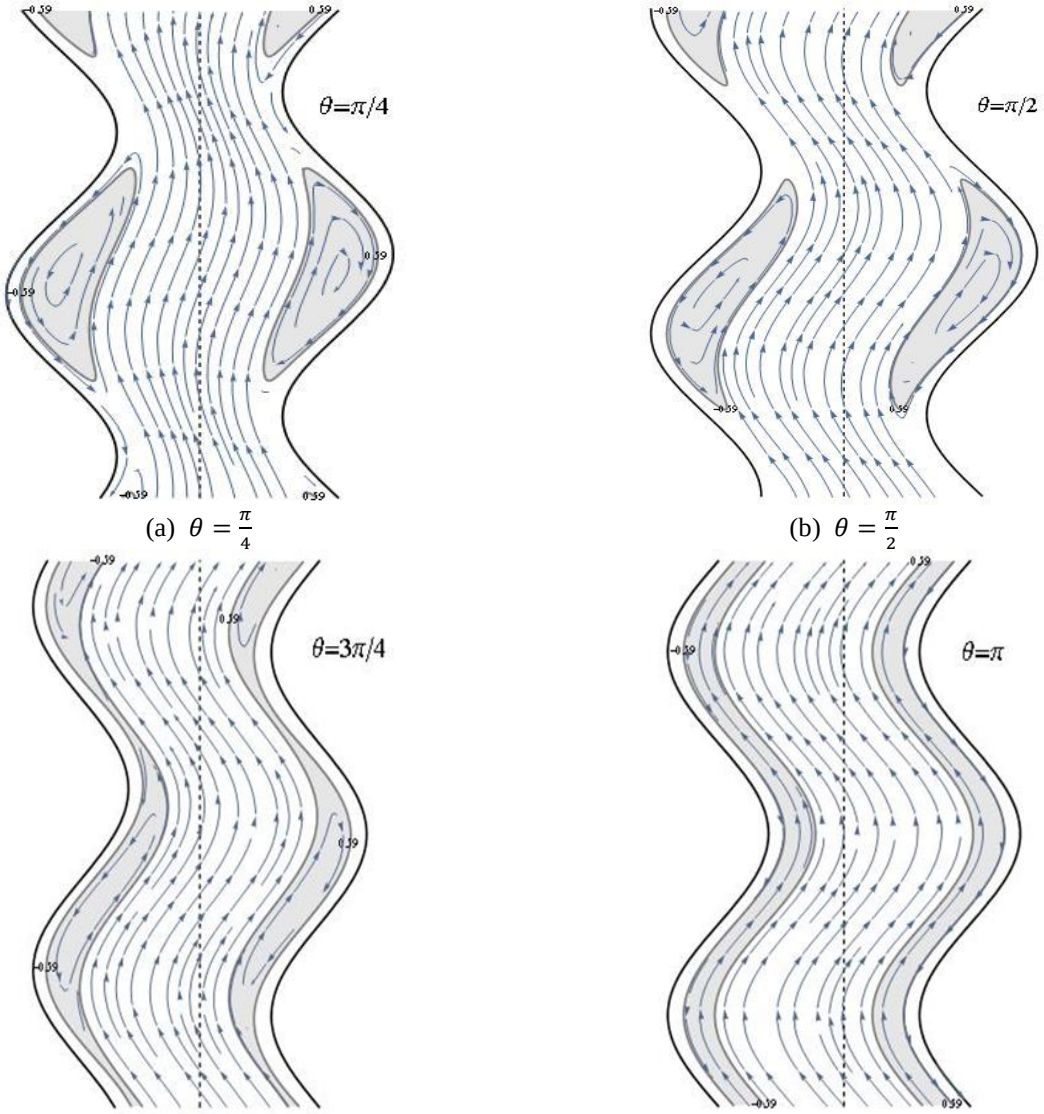

(a) $\theta = \frac{\pi}{4}$ (b) $\theta = \frac{\pi}{2}$

(c) $\theta = \frac{3\pi}{4}$ (d) $\theta = \pi$

Fig. 11 Effect of phase angle θ in trapping phenomena with $\xi = 1.0, B_r = 0.1, \sigma_r = 1, k_r = 100, (\rho\alpha)_r = 1, M = 0, K = 1, R_n = 1\ \nu = 1.0, \bar{Q} = 3.0,$ and $G_r = 0$

values, and the spherical shape gives the greatest effect on heat distribution.

• The higher the value of the magnetic parameter, the more closely the effect of increasing the radiation parameter will be on the heat distribution.

• The two boluses disappear at $\theta = \pi$ so that there is no trapping at it.

7. Future work

This study assumes, that only the thermal radiation parameter R_n combined with some parameters such as ξ, G_r, $\bar{Q}$ and M are investigated; however, investigating the impact of the Brinkman number B_r is far from the aims of the current study. The reflux phenomenon is not included in the current study so all of them are recommended for future work.

References

Ahmadi Azar, A., Jalili, B., Jalili, P. and Ganji, D.D. (2023), "Investigating the effect of structural changes of two stretching disks on the dynamics of the MHD model", *Sci. Rep.*, **13**(1), 1-19. https://doi.org/10.1016/j.devcel.2021.06.008

Ahmed, B., Hayat, T., Muhammad,k. and Alsaedi, A. (2023), "MHD peristaltic activity of powell-eyring nanomaterial through porous space with slip effects", *Case Stud. Therm. Eng.*, **45**. https://doi.org/10.1016/j.csite.2023.103001.

Ahmed, B., Hayat,T., Abbasi, F.M. and Alsaedi, A. (2021), "Mixed convection and thermal radiation effect on MHD peristaltic motion of Powell-Eyring nanofluid", *Int. Commun. Heat Mass Transf.*, **126**. https://doi.org/10.1016/j.icheatmasstransfer.2021.105320.

Ahmed, B., Liu, D., Zhang, Y. and Hussien, M.A. (2024), "Peristaltic pumping of convective nanofluid with magnetic field and thermal radiation in a porous channel", *Case Stud. Therm. Eng.*, **53**. https://doi.org/10.1016/j.csite.2023.103918.

Azam, M. (2022), "Effects of Cattaneo-Christov heat flux and nonlinear thermal radiation on mhd maxwell nanofluid with

arrhenius activation energy", *Case Stud. Therm. Eng.*, **34**. https://doi.org/10.1016/j.csite.2022.102048.

Daryayehsalameh, B., Ayari,M.A., Tounsi,A., Khandakar,A. and Vaferi,B. (2022), "Differentiation among stability regimes of Alumina-Water nanofluids using smart classifiers", *Adv. Nano Res.*, **12**(5), 489-499. https://doi.org/10.12989/anr.2022.12.5.489.

Eldabe, N.T., Asar, A.S. and Shawky, H.M. (2020). "Effects of slip velocity and hall currents on peristaltic transport of Bingham-Papanastasiou fluid with heat transfer", *Appl. Math. Inf. Sci.*, **14**(1), 31-40. https://doi.org/10.18576/AMIS/140104.

Gharsseldien, Z. M. and Awaad, A.S. (2022), "Maxwell nanofluid flow through a heated vertical channel with peristalsis and magnetic field", *Adv. Nano Res.*, **13**(1), 77-86. https://doi.org/10.12989/anr.2022.13.1.077.

Gharsseldien, Z.M., Mekheimer, Kh.S. and Awad, A.S. (2010), "The influence of slippage on trapping and reflux limits with peristalsis through an asymmetric channel", *Appl. Bionics. Biomech.*, **7**(2), 95-108. https://doi.org/10.1080/11762321003747099.

Hamilton, R.L. (1962), "Thermal conductivity of heterogeneous two-component systems", *Ind. Eng. Chem. Fundam.*, **1**(3), 187-191. https://doi.org/10.1021/i160003a005.

Hussain, M., Sharif, H., Khadimallah, M.A., Mouldi,A., Loukil, H., Ali, M.R. and Tounsi, A. (2023), "Shooting method applied to porous rotating disk: Darcy-Forchheimer flow of nanofluid", *Adv. Nano Res.*, **14**(3), 295-302. https://doi.org/10.12989/anr.2023.14.3.295.

Iqbal, J., Abbasi, F.M., Alkinidri, M. and Alahmadi, H. (2023), "Heat and mass transfer analysis for MHD bioconvection peristaltic motion of Powell-Eyring nanofluid with variable thermal characteristics", *Case Stud. Therm. Eng.*, **43**. https://doi.org/10.1016/j.csite.2022.102692.

Jafaripournimchahi, A., Shateri, A., Jalili, B., Jalili, P., Ganji, D.D. (2024), "The effects of magnetic field and thermal radiation on the mixed convection of Al2O3-Cu/water hybrid nanofluid over a permeable vertical flat plate", *Mod. Phys. Lett. B.*, 2450242. https://doi.org/10.1142/S0217984924502427

Kazemia, M.H. and Nasr, M.A.B.M. (2014), "Convective heat transfer of MWCNT / HT-B oil nanofluid inside micro-fin helical tubes under uniform wall temperature condition", *Adv. Nano Res.*, **2**(2), 99-109. https://doi.org/10.12989/anr.2014.2.2.099.

Kodi, R., Ganteda, C., Dasore, A., Kumar, M.L., Laxmaiah, G., Hasan, M.A., Islam, A. and Razak, A. (2023), "Influence of MHD mixed convection flow for maxwell nanofluid through a vertical cone with porous material in the existence of variable heat conductivity and diffusion", *Case Stud. Therm. Eng.*, **44**. https://doi.org/10.1016/j.csite.2023.102875.

Mirzaei, A., Jalili, P., Afifi, M.D., Jalili, B. and Ganji, D.D. (2023), "Convection heat transfer of MHD fluid flow in the circular cavity with various obstacles: finite element approach", *Int. J. Thermofl.*, **20**. https://doi.org/10.1016/j.ijft.2023.100522.

Noreen, S. (2018), "Peristaltically assisted nanofluid transport in an asymmetric channel.", *Karbala Int. J. Mod. Sci.*, **4**(1), 35-49. https://doi.org/10.1016/j.kijoms.2017.10.005.

Rafiq, M., Yasmin, H., Hayat, T. and Alsaadi,F. (2019), "Effect of hall and ion-slip on the peristaltic transport of nanofluid: A biomedical application", *Chin. J. Phys.*, **60**, 208-227. https://doi.org/10.1016/j.cjph.2019.04.016.

Rezaee, M., Yeganegi, A., Namvarpour, M. and Ghassemi, H. (2022), "Fluid flow dynamics in deformed carbon nanotubes with unaffected cross-section", *Adv. Nano Res.*, **12**(3), 253-261. https://doi.org/10.12989/anr.2022.12.3.253.

Shah, S., Rafiq,N., Abdullah, F.A., Atif, S.M. and Abbas, M. (2022), "Slip and radiative effects on MHD Maxwell nanofluid with non-Fourier and non-Fick laws in a porous medium", *Case Stud. Therm. Eng.*, **30**. https://doi.org/10.1016/j.csite.2022.101779.

Sharif, H., Khadimallah, M.A., Naeem, M.N., Hussain, M., Hussain, S. and Tounsi, A. (2021), "Flow of MHD Powell-Eyring nanofluid: heat absorption and Cattaneo-Christov heat flux model", *Adv. Nano Res.*, **10**(3). https://doi.org/10.12989/anr.2021.10.3.221.

Sheikholeslami, M., Gorji-Bandpy, M., Ganji, D.D. and Soleimani, S. (2014), "Heat flux boundary condition for nanofluid filled enclosure in presence of magnetic field", *J. Mol. Liq*, **193**, 174-184. https://doi.org/10.1016/j.molliq.2013.12.023.

Sheikholeslami, M., Gorji-Bandpy, M., Ganji, D.D., Soleimani, S. and Seyyedi, S.M. (2012), "Natural convection of nanofluids in an enclosure between a circular and a sinusoidal cylinder in the presence of magnetic field", *Int. Commun. Heat Mass Transf.*, **39**(9), 1435-1443. https://doi.org/10.1016/j.icheatmasstransfer.2012.07.026.

Sheikholeslami, M. and Ganji, D.D.. (2017), *Applications of Nanofluid for Heat Transfer Enhancement*, Elsevier Ltd., New York, U.S.A.

Sobamowo, M.G., Yinusa, A.A. and Oluwo, A.A., (2018), "Slip analysis of magnetohydrodynamics flow of an upper-convected Maxwell viscoelastic nanofluid in a permeable channel embedded in a porous medium", *Aeronaut. Aerosp. Open Access J.*, **2**(5). https://doi.org/10.15406/aaoaj.2018.02.00065.

Turns, S.R. and Kraige, D.R. (2007), *Property Tables for Thermal Fluids Engineering*, Cambridge University Press, New York, U.S.A.

Vajravelu, K., Sreenadh, S. and Lakshminarayana, P. (2011), "The influence of heat transfer on peristaltic transport of a Jeffrey fluid in a vertical porous stratum", *Commun. Nonlinear Sci. Numer. Simul.*, **16**(8), 3107-3125. https://doi.org/10.1016/j.cnsns.2010.11.001.

Vijay, N. and Sharma, K., (2023), "Dynamics of stagnation point flow of Maxwell nanofluid with combined heat and mass transfer effects: a numerical investigation", *Int. Commun. Heat Mass Transf.*, **141**. https://doi.org/10.1016/j.icheatmasstransfer.2022.106545.

Zainal, N.A., Nazar, R., Naganthran, K. and Pop, I., (2022), "The impact of thermal radiation on maxwell hybrid nanofluids in the stagnation region", *Nanomater.*, **12**(7). https://doi.org/10.3390/nano12071109.

CC

Nomenclature

C_f	Specific heat of the fluid
$\boldsymbol{V}$	Fluid velocity vector
P	The pressure
$\boldsymbol{F}$	The body force
T	Temperature
$\boldsymbol{q}_r$	The radiation heat flux vector
$\boldsymbol{J}$	The total current density
$\boldsymbol{R}$	Darcy's resistance
K	The permeability parameter
k_0	The Rosseland mean absorption coefficient.
M	The Hartmann number
R_e	The Reynolds number

ρ_{nf}	The density of the nanofluid
$(\rho C)_{nf}$	The heat capacity of the nanofluid
k_{nf}	The thermal conductivity of the nanofluid
λ_1	The fluid relaxation time
μ_{nf}	The kinematic viscosity coefficient of the nanofluid
λ	The wavelength
σ_{nf}	The electric conductivity
σ_0	Stefan-Boltzman constant
α_{nf}	The thermal expansion coefficient of nanofluid.
Θ	The dimensionless temperature,
μ_f	The kinematic viscosity coefficient of the fluid
ϕ	The nanoparticle volume fraction
ξ	Nanoparticle shape parameter (sphericity)